

NanoScience and Technology

Patrick Vogt · Guy Le Lay *Editors*

Silicene

Prediction, Synthesis, Application

 Springer

NanoScience and Technology

Series editors

Phaedon Avouris, IBM Research, Yorktown Heights, USA

Bharat Bhushan, The Ohio State University, Columbus, USA

Dieter Bimberg, Technical University of Berlin, Berlin, Germany

Cun-Zheng Ning, Arizona State University, Tempe, USA

Klaus von Klitzing, Max Planck Institute for Solid State Research, Stuttgart,
Germany

Roland Wiesendanger, University of Hamburg, Hamburg, Germany

Patrick Vogt · Guy Le Lay
Editors

Silicene

Prediction, Synthesis, Application

 Springer

Editors

Patrick Vogt
Institut für Physik
Technische Universität Chemnitz
Chemnitz, Germany

Guy Le Lay
CNRS, PIIM UMR 7345
Aix-Marseille University
Marseille, France

ISSN 1434-4904 ISSN 2197-7127 (electronic)
NanoScience and Technology
ISBN 978-3-319-99962-3 ISBN 978-3-319-99964-7 (eBook)
<https://doi.org/10.1007/978-3-319-99964-7>

Library of Congress Control Number: 2018953713

© Springer Nature Switzerland AG 2018

This work is subject to copyright. All rights are reserved by the Publisher, whether the whole or part of the material is concerned, specifically the rights of translation, reprinting, reuse of illustrations, recitation, broadcasting, reproduction on microfilms or in any other physical way, and transmission or information storage and retrieval, electronic adaptation, computer software, or by similar or dissimilar methodology now known or hereafter developed.

The use of general descriptive names, registered names, trademarks, service marks, etc. in this publication does not imply, even in the absence of a specific statement, that such names are exempt from the relevant protective laws and regulations and therefore free for general use.

The publisher, the authors, and the editors are safe to assume that the advice and information in this book are believed to be true and accurate at the date of publication. Neither the publisher nor the authors or the editors give a warranty, express or implied, with respect to the material contained herein or for any errors or omissions that may have been made. The publisher remains neutral with regard to jurisdictional claims in published maps and institutional affiliations.

This Springer imprint is published by the registered company Springer Nature Switzerland AG
The registered company address is: Gewerbestrasse 11, 6330 Cham, Switzerland

Chapter 1

A Vision on Organosilicon Chemistry and Silicene



Deepthi Jose, Chandra Chowdhury and Ayan Datta

Abstract Replacement of carbon atoms from aromatic molecules and their two-dimensional extended analogues (graphene) have been predicted to have interesting structural diversity and tunable electronic properties. Recent progress in the experimental realization of such systems is discussed along with a conceptual understanding of the structural properties of planar organosilicon compounds and silicene. Pseudo Jahn-Teller (PJT) distortion is shown to contribute to the buckling distortions in silicene which make them excellent materials for band-gap tuning through hydrogenation. Chemical doping of silicene by cations is suggested to be a strategy to suppress buckling of silicene and regain its perfect planar two-dimensional silicon framework. TERS spectroscopy is proposed as a tool to probe the presence or absence of buckling distortions in silicene and cation doped silicene respectively.

1.1 Aromatic Molecules and Silicon Substituted Cyclic Rings

The concept of aromaticity or the special stability of cyclic π -conjugated molecules occupies a special position in chemistry. Such molecules are associated with their unusual stability. Manifestation of this stability is seen in their reluctance to undergo several reactions like hydrogenation and oxidation which are much more facile for non-conjugated cyclic molecules. Structurally these molecules are symmetric and vibrationally stable towards distortions to lower symmetry configurations [1]. In 1930s, Hückel proposed a simple model analogous to the tight-binding model popular in solid-state physics for simple cyclic π -conjugated molecules and proposed that

D. Jose

Department of Chemistry, Providence Women's College, Calicut 673009, Kerala, India
e-mail: alphydeepthi@gmail.com

C. Chowdhury · A. Datta (✉)

Department of Spectroscopy, Indian Association for the Cultivation of Science, Jadavpur 700032, West Bengal, India
e-mail: spad@iacs.res.in

© Springer Nature Switzerland AG 2018

P. Vogt and G. Le Lay (eds.), *Silicene*, NanoScience and Technology,
https://doi.org/10.1007/978-3-319-99964-7_1

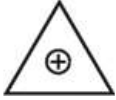

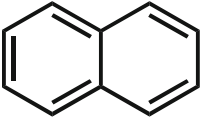
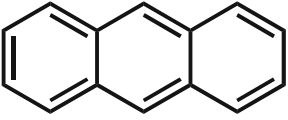
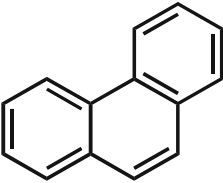

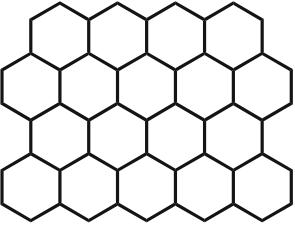
cyclic molecules with $(4n + 2) \pi$ electrons (where $n = 0, 1, 2, \dots$) should be stabilized due to aromaticity [2–4]. As shown in Table 1.1, several such molecules with integer multiples of n have been synthesized chemically and characterized by various spectroscopic tools. Of particular mention should be the X-Ray diffraction studies that have shown that these structures are highly symmetric and the bond length alterations (BLA, Δr) are typically less than 1–2%. The concept of stitching small aromatic molecules in-plane to generate massive two-dimensional graphene like two dimensional materials has been achieved experimentally. Müllen and co-workers have designed atomistically precise graphene nanoribbons based on bottom up synthesis starting from a simple anthracene molecule [5] (linear ($n = 3$) in Table 1.1).

Therefore, for generating two dimensional silicon analogue of benzene namely silicene, one should have a clear understanding of small benzene like silicon rings which might be fused to generate large silicene flakes. In fact, it is with this aim that several groups have pursued the synthesis of silicon substituted aromatic and fused aromatic systems.

In Fig. 1.1, we enlist the experimentally synthesized silicon substituted aromatic molecule. Such sila-aromatic molecules are kinetically labile towards atmospheric oxidation. Therefore, a general experimental strategy to synthesize such molecules has been to use bulky protecting groups which create hydrophobic pockets around these molecules. Tokitoh and co-workers have synthesized silabenzene and silanaphthalene [6, 7] (structures 1(a), 1(b)) and B3LYP/6-31G(d) calculations have revealed that there is a small energy difference between Dewar silabenzene and silabenzvalene, while the planar silabenzene is by far the most stable among the isomers. Jutzi et al. have synthesized the 1,1-dimethyl SiC_5H_5 anion (structure 1(c)) which based on structural and qualitative molecular orbital theory calculations has been shown to be aromatic [8]. Sasamori and co-workers have synthesized 9-silaphenanthrene. Crystal structure analysis of 9-silaphenanthrene have shown that the structure remains planar (structure 1(d)) [9]. Based on NMR chemical shifts and NICS calculations, the authors concluded that 9-silaphenanthrene has delocalized 14π electron aromatic configuration. Tanabe et al. have synthesized 1,1'-Disila-4,4'-biphenyl (structure 1(e)) [10]. X-ray studies show that both the phenyl rings remain planar and the twist angle of the central C-C bonds between the silaaromatic rings are 41° which is similar to that of biphenyl (45°). The UV-vis spectrum of 1,1'-Disila-4,4'-biphenyl showed a red shift and a massive six times enhancement in absorbance compared to that of Tbt-substituted silabenzene. This therefore suggests the existence of extended conjugation through the single bond connecting two silaaromatic rings, a concept well-known in the realms of carbon based on aromatic systems.

A significant experimental achievement in this area has been the synthesis of an isomer of hexasilabenzene by Abersfelder and co-workers [11]. They synthesized dark green crystals of an isomer of Si_6R_6 ($\text{R} = \text{Tip}, 2, 4, 6\text{-triisopropylphenyl}$ and $2, 6\text{-diisopropylphenyl}$) by the reduction of unsymmetrically substituted trichlorocyclotrisilane (see Fig. 1.2). It has a chair-like conformation in accordance with the theoretical results [12, 13]. Authors propose the term dismutational aromaticity to explain the bonding pattern of this molecule. In order to quantify the aromaticity of the molecule, they calculated the nucleus-independent chemical shift, NICS(0),

Table 1.1 Existence cyclic stable molecules in line with the predictions from the Hückel model

n	Molecule	Structure and Symmetry
0	Cyclopropyl cation	 D_{3h}
1	Benzene	 D_{6h}
2	Naphthalene	 D_{2h}
3	Anthracene (linear)	 D_{2h}
3	Phenanthrene (bent)	 C_{2v}
6	Coronene (circular) (Hückel antiaromatic)	 D_{6h}
∞	Graphene (flat 2D lattice)	 C_s

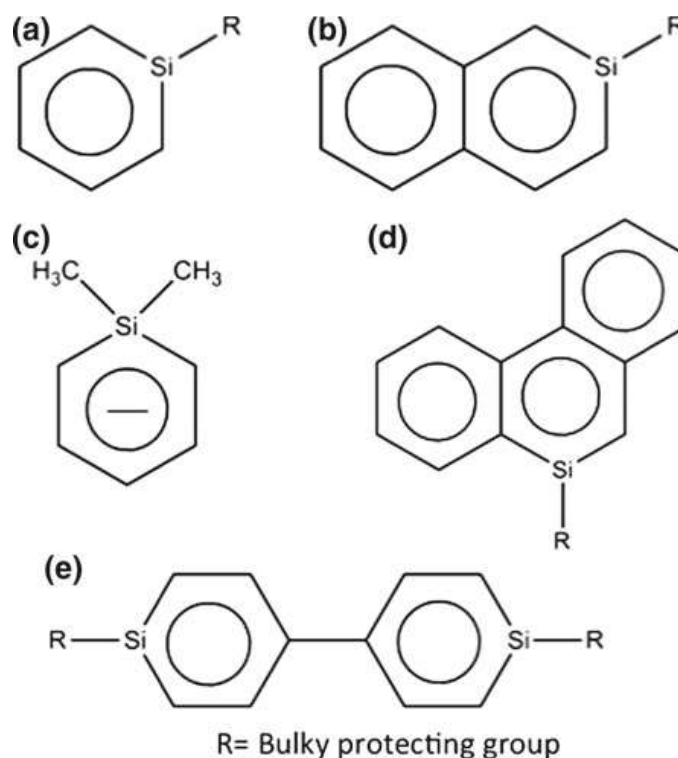


Fig. 1.1 Experimentally synthesized Sila-aromatic molecules

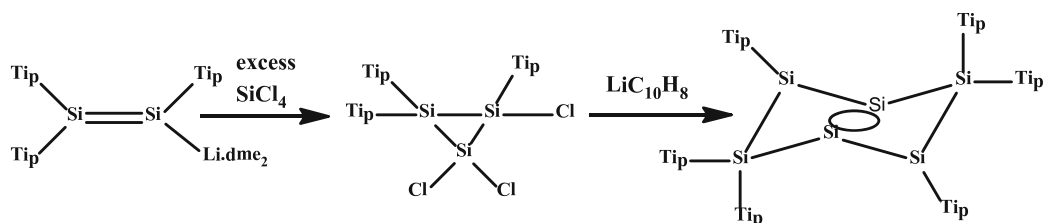


Fig. 1.2 Synthesis of the tricyclic isomer of hexasilabenzene (Tip: 2,4,6-triisopropylphenyl; Li.dme₂: 1,2-dimethoxyethane solvated Li)

at the center of the Si₄ ring (−23.8 ppm), which indicates substantial aromaticity (benzene ~ −10 ppm) but may also include shielding effects from the σ-framework. To estimate these latter effects, they also computed the NICS(0) value for the hypothetical saturated hydrogenation product of the molecule, Si₆R₆H₆. This *in silico* reduction has the effect of sequestering the two Si lone pair electrons and hence suppressing the dismutational resonance. The result (−6.4 ppm) suggests that the strongly diatropic NICS(0) value of Si₆R₆ is truly due to aromaticity.

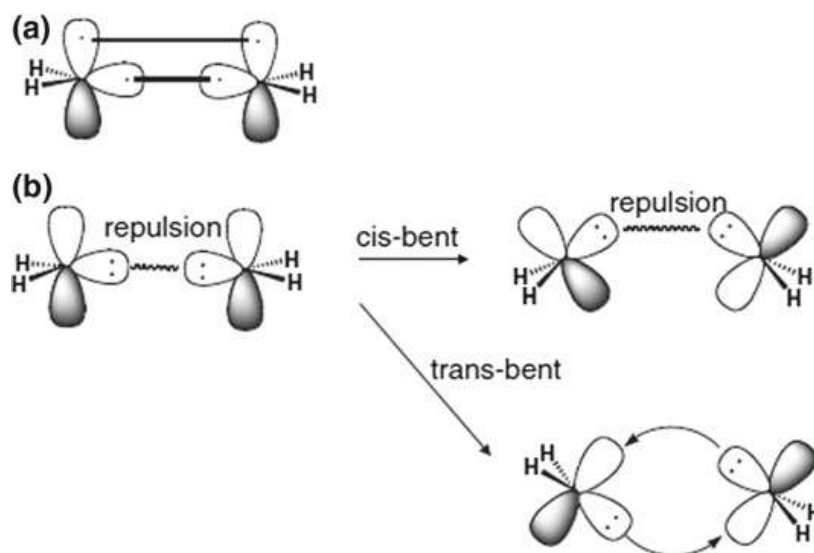


Fig. 1.3 a Bonding in planar $\text{H}_2\text{C}=\text{CH}_2$ b Bonding in trans-bent $\text{H}_2\text{Si}=\text{SiH}_2$. Reproduced with permission from [14]

1.2 Chemical Bonding: Unsaturated Carbon Systems Versus Silicon Systems

The contrasting behavior of the unsaturated carbon systems and their heavier analogues have been discussed in details by Nagase recently [14]. Here we mention the basic features which lead to different structures in silicenes and other two dimensional materials.

One might envision bonding in $\text{CH}_2=\text{CH}_2$ or higher unsaturated organic molecules as composed of interaction between two or more CH_2 fragments. As shown in Fig. 1.3a, each of these CH_2 units have two unpaired electrons ($S = 1$, triplet). These two unpaired electrons are located in a hybridized sp^2 orbital and a perpendicular p_z orbital respectively. So, as these fragments are brought closer, a maximum overlap between these two orbitals occurs when the overall $\text{H}_2\text{C}=\text{CH}_2$ unit adapts a perfectly planar configuration (a D_{2h} point group). However, this case is altered in Silicon hydrides. The ground state of SiH_2 does not contain unpaired electrons ($S = 0$, singlet). So, the two free electrons pair up and are localized as a lone-pair in the sp^2 hybrid orbital (Fig. 1.3b). Hence, now approach of the two SiH_2 units along the shortest path should lead to strong electron-electron repulsion between the two filled orbitals. The only way to form a $\text{H}_2\text{Si}=\text{SiH}_2$ bond will be to distort the structure either in a *cis-bent* or a *trans-bent* fashion. Clearly, a *cis-bent* structure should still possess this repulsion albeit in a relatively weaker angular fashion. Therefore, the best orientation of the $\text{H}_2\text{Si}=\text{SiH}_2$ unit is the distorted *trans-bent* structure. It is important to remember that even though the $\text{H}_2\text{Si}=\text{SiH}_2$ bond has a formal bond order of two, the *trans-bent* distortion leads to a weaker and hence, relatively longer double bonded system.

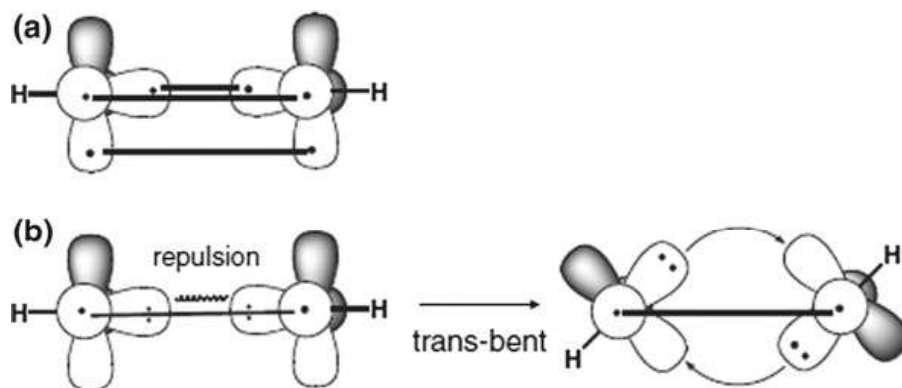


Fig. 1.4 a Bonding in linear HC≡CH b Bonding in trans-bent HSi≡SiH. Reproduced with permission from [14]

Similar to the ethylenic units, the silicon substituted acetylenes, HSi≡SiH also have a *trans-bent* structure. For both CH and SiH, the ground state has one unpaired electron ($S = 1/2$, doublet). However, for CH, the excitation energy required to possess three unpaired electrons ($S = 3/2$, quartet) is very small (~ 16.7 kcal/mol). Hence, the CH unit undergoes excitation to reach to a quartet state which facilitates it form three carbon-carbon (one σ and two π) bonds. This results in a gain in binding energy of 228.5 kcal/mol, a more than ten fold gain compared to the loss in terms of the excitation energy. The formation of a triple bond in HE≡EH is shown schematically in Fig. 1.4a. This results in linear HC≡CH molecule ($D_{\infty h}$ point group). For SiH, the doublet-quartet excitation energy is much more (~ 36.4 kcal/mol). Also, the strength of a linear triple bonded HSi≡SiH is expected to be smaller due to poor overlap between the two diffused $3p_z$ orbitals (formation of one σ bond) and two diffused $3p_x$ and $3p_y$ (formation of two π bond, perpendicular to the σ bond and with respect to each other). Therefore, the SiH units prefer to react by orienting their lone-pairs as far as possible as with respect to each other resulting in a *trans-bent* structure as shown in Fig. 1.4b.

One might understand the preference of the HSi≡SiH systems to possess *trans-bent* geometries from the pseudo Jahn-Teller effects (PJTE) [15–17]. As shown in Fig. 1.5, formation of a triple bonded HE≡EH unit ($E=C, Si$) involves filling up of a pair of electrons in one σ -orbital and two pairs of electrons in the in-plane (π_{in}) and out of plane (π_{out}) orbitals of π -symmetry. Distortion along the *trans-bent* normal mode, $Q(\pi_g)$ leads to a symmetry allowed mixing of the filled π_{in} orbital (π_u symmetry) and the empty σ^* orbital (σ_u symmetry). In the case of C_2H_2 , calculations at B3LYP/aug-cc-PVTZ level show that the energy separation between the π_{in} orbital and the σ^* orbital is 8.4 eV making this interaction extremely weak to effectively result in a structural distortion. However, for Si_2H_2 , the $\pi_{in}-\sigma^*$ gap is only 3.6 eV at the same level of theory. This causes structural instability for the $D_{\infty h}$ linear structure in Si_2H_2 with an imaginary distortion mode ($\omega_{\pi_g} = 610.8i$ cm^{-1}) which on relaxation leads to the *trans-bent* structure of Si_2H_2 of a lower C_{2h} symmetry. Therefore, a small gap between the filled state (occupied molecular orbital,

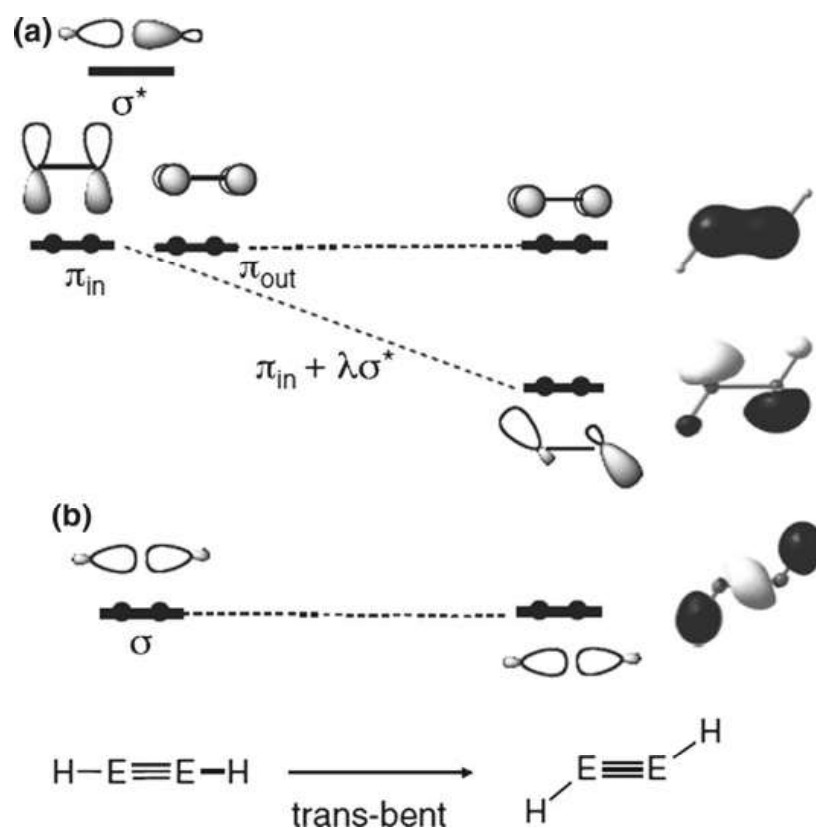


Fig. 1.5 a Bonding in linear $HC\equiv CH$ b Bonding in trans-bent $HSi\equiv SiH$. Reproduced with permission from [14]

OMO) and the empty state (unoccupied molecular orbital, UMO) leads to structural instability in linear $HSi\equiv SiH$ systems. Such distortions belong to the general class of molecular distortions arising out of small OMO-UMO gaps, a *prime-facie* condition for PJT distortions. In fact, the preference for various heavier analogues of benzene like hexasilabenzene and hexagermanabenzene to have a distorted D_{3d} geometry instead of the expected planar D_{6h} geometry has been explained by us based on PJT effect [18]. We discuss this in details in the next section.

1.3 Effect of Buckling Distortions in Si_6 Rings: The Psuedo Jahn-Teller (PJT) Effect

Ab initio calculations predict buckled honeycomb geometry for silicene unlike graphene even though it possess similar electronic properties [19, 20]. The symmetry breaking in silicenes by buckling removes the instability associated with the planar high-symmetry structure. Such an instability of high-symmetry geometries of molecular systems is attributed to pseudo-Jahn-Teller (PJT) effect [15, 16]. As suggested by Bersuker, the vibronic coupling between the nondegenerate electronic

states of proper symmetry resulting in nonsymmetric vibrations leads to PJT effect [17, 21, 22]. The sufficiently strong coupling between the unoccupied molecular orbitals (UMOs) with occupied molecular orbitals (OMOs) has been identified and proved to be the source of distortions in many molecular systems [17, 23, 24]. The PJT effect can be suppressed by adding electrons to the UMOs, by increasing the energy gap between the interacting UMO and OMO, or by the isolobal substitution of atom or a group with their more electronegative analogues [25–27]. Puckering in silicene makes it more versatile since, besides having all the exotic properties of graphene, tuning the band gap is much easier [28, 29]. Unlike the ripples in graphene, which are disordered, silicene is puckered in each of the six membered ring and is symmetric across the surface. Because this short-range puckering has a pronounced effect on the electronic properties of silicene it is important to explore the fundamental aspects of puckering distortions and the factors that lead to puckering in silicene. A proper understanding of the buckling distortions is crucial to appreciate the novel properties of silicene and to tune it for various applications.

The silicene clusters gain stability on puckering with increase in the number of rings from Si_6H_6 to $\text{Si}_{70}\text{H}_{22}$ [30]. As shown in Fig. 1.6, the puckering angle ϕ (the dihedral angles between the atoms 1, 2, 3, and 4) for the optimized geometry of Si_6H_6 at B3PW91/TZVP is 33.7° and that for $\text{Si}_{70}\text{H}_{22}$ is 35.6° . Periodic calculations for silicene using VASP plane wave based DFT code find the puckering angle for the optimized silicene sheet is about 36.8° (part c of Fig. 1.6). The puckering distortion in the smallest silicene cluster hexasilabenzene is preserved as such in silicene sheets. The structure, stability and aromaticity of isomers of hexasilabenzene has been studied extensively by various research groups [12, 31, 32]. Among the various isomers hexasilaprismane is computed to be the global minimum in the potential energy surface. The silicon analogue of benzene is 22.7 kJ/mol less stable than hexasilaprismane at CCSD(T)/cc-pVTZ level [33]. Because this D_{3d} structure is the smallest puckered repeating unit for silicene clusters and sheets, we chose chairlike hexasilabenzene for understanding the puckering distortions.

The strong vibronic coupling of nondegenerate orbitals that are sufficiently close in energy leads to vibrational instability in high symmetry configurations. The symmetry requirement for PJT effect is that the direct product of the symmetries of the nondegenerate orbitals should contain the symmetry of the instability path [34]. The onset of new covalence when a high symmetric configuration moves to a low symmetry configuration is responsible for PJT effect. Its well established in the literature that the planar hexasilabenzene is not a minimum energy isomer and has a vibrational instability (128.8i at M05-2X/6-31 + G(d,p) level of theory) that leads to a C_3 puckered structure [12, 31]. The Si–Si bond length increases from 2.21 to 2.23 Å as hexasilabenzene gets puckered, which is still less than the single Si–Si bond length of 2.35 Å. The planar hexasilabenzene is in $^1A_{1g}$ electronic structure. The distortion along the unstable b_{2g} vibrational mode results in the chairlike D_{3d} structure and the b_{2g} mode becomes totally symmetric (a) mode. The vibronic coupling between the OMO-UMO pairs: HOMO and LUMO+2, HOMO-1 and LUMO+3 and/or HOMO-4 and LUMO can lead to the distortion of the D_{6h} structure. The product of the symmetries of OMO-UMO orbitals are:

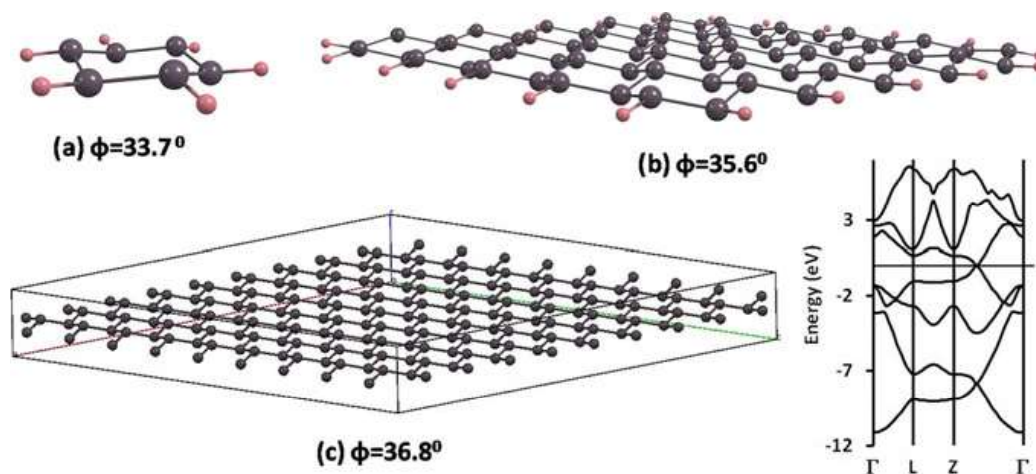


Fig. 1.6 Puckering Angle ϕ for **a** Si_6H_6 , **b** Large 2D molecular fragment: $\text{Si}_{70}\text{H}_{22}$, and **c** Infinite 2D Silicene Sheet with the computed band structure exhibiting the Dirac Cone. Reproduced with permission from [18]

$$\text{HOMO and LUMO} + 2: e_{1g} \times e_{2g} = b_{1g} + b_{2g} + e_{1g}$$

$$\text{HOMO-1 and LUMO} + 3: a_{2u} \times b_{1u} = b_{2g}$$

$$\text{HOMO-4 and LUMO}: e_{1u} \times e_{2u} = b_{1g} + b_{2g} + e_{1g}.$$

The energy gap between these OMO-UMO pairs are 6.83, 8.90, and 9.52 eV, respectively. The vibronic coupling in the OMO-UMO pairs HOMO-1 and LUMO+3 and HOMO-4 and LUMO can be neglected because the energy gap is significantly high. As shown in part a of Fig. 1.7, the PJT distortion due to the coupling between HOMO and LUMO+2 orbitals leads to the puckered D_{3d} geometry of hexasilabenzene. In the case of planar hexasilabenzene, the overlap of σ and π orbitals is zero. But puckering leads to σ - π mixing resulting in a new covalence.

1.4 Chemical Functionalization on Silicon Rings to Make Them Planar

The cation- π interactions are widespread and have considerable significance in molecular biology, drug discovery, and supramolecular chemistry [35, 36]. Experimental and theoretical investigations have shown that the cation- π binding energies depend on the substituents on the aromatic surface and position and electronegativity of the cation [37, 38]. The origin of cation- π interactions in benzene and other aromatic molecules has been mainly attributed to the electrostatic interaction and induction energy [39, 40]. Sergeeva et al. have reported the flattening of pentasilacyclopentadienide ring by suppressing pseudo Jahn-Teller effect using Mg^{2+} ions [26]. Ab initio calculations by Zdzetsis predict that Si_6 can be made planar through

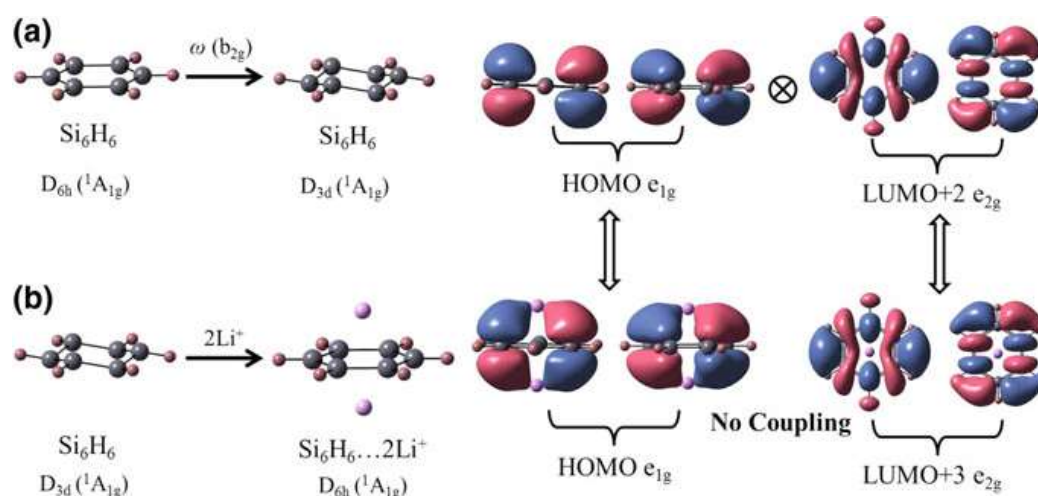


Fig. 1.7 **a** Onset of puckering from $D_{6h} \rightarrow D_{3d}$ via b_{2g} distortion in hexasilabenzene. The corresponding OMO and UMO involved in this vibronic mixing associated PJT are also shown. **b** Suppression of distortion in hexasilabenzene $\cdots 2\text{Li}^+$. The 1–1 correspondence between the OMO and UMO are shown with respect to the undoped hexasilabenzene. (Calculations were done at M05-2X/6-31+g(d,p) level.) Reproduced with permission from [18]

the reduction of Si_6^{6-} anion in the presence of counter cations. The resulting Si_6Li_6 is planar, stable, and aromatic [41]. We performed DFT calculations to investigate whether the π -surface of hexasilabenzene can bind a metal ion. In the presence of Li^+ , the puckered Si_6 ring of hexasilabenzene becomes planar to form a stable C_{6v} $\text{Si}_6\text{H}_6 \cdots \text{Li}^+$ complex. The BSSE corrected binding energy for hexasilabenzene with Li^+ is -45.3 kcal/mol. The corresponding value for benzene $\cdots \text{Li}^+$ complex is -39.9 kcal/mol. The distance between the metal ion and the centroid of the ring is 1.94 Å. Li^+ ion not only binds with hexasilabenzene more strongly than benzene but also suppresses the PJT distortion in hexasilabenzene ring. The energy gap of the OMO-UMO pair of hexasilabenzene increased from 6.83 to 7.37 eV in the presence of a Li^+ ion. The increase in energy gap in presence of Li^+ is sufficient enough to quench the coupling of OMO-UMO pair thereby suppressing the PJT effect along the b_{2g} mode. The π -surface of aromatic rings can be tuned to accommodate two cations [42]. We calculated the binding energy of hexasilabenzene with two Li^+ ions. Unlike benzene for which binding of two cations on either side of the aromatic ring is endothermic, hexasilabenzene forms a stable D_{6h} $\text{Si}_6\text{H}_6 \cdots 2\text{Li}^+$ complex and the BSSE corrected binding energy is -3.5 kcal/mol. The distance between the metal ion and the centroid of the ring is 2.18 Å. The electrostatic field from the two Li^+ ions increases the OMO-UMO energy gap to 7.68 eV restoring high symmetry D_{6h} structure of hexasilabenzene. Part b of Fig. 1.7 shows the suppression of PJT distortion of hexasilabenzene in the presence of two Li^+ ions. The one-to-one correspondence between the OMO and UMO of hexasilabenzene and the 2:1 Li^+ doped hexasilabenzene are also shown.

Inspired by the results for planarization for hexasilabenzene on mono and di lithiation, material with planar silicene sheet decorated with Li^+ were designed and

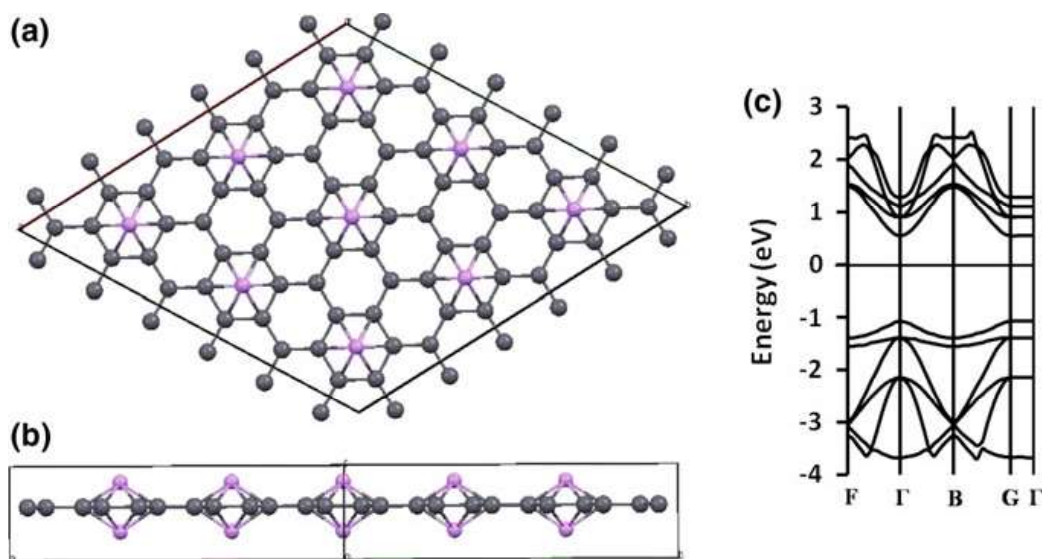


Fig. 1.8 **a** Transverse view, **b** lateral view of optimized Li^+ -decorated silicene sheet, **c** its band structure (at the GGA/PBE level with plane wave basis). Reproduced with permission from [18]

periodic calculations were performed for such extended system. The unit cell was constructed such that the Li^+ ions bind to the top and bottom surface of alternate hexasilabenzene ring. In agreement with the results of hexasilabenzene, the silicene sheet turns planar in the presence of Li^+ ions. The transverse and lateral view of a 3×3 supercell of the optimized Li^+ decorated silicene cluster is shown in Fig. 1.8. The presence of Li^+ ions open up the band gap in silicene (part c of Fig. 1.5). The band gaps for silicene $\cdots\text{Li}^+$ and silicene $\cdots 2\text{Li}^+$ are calculated to be 1.29 and 1.25 eV, respectively. The band gaps are estimated to be 1.70 and 2.14 eV (1.62 and 2.10 eV) at HSE06 and B3LYP hybrid levels of calculations for silicene $\cdots\text{Li}^+$ (silicene $\cdots 2\text{Li}^+$), respectively.

1.5 Electron and Hole Transport in Silicene

The Reorganization Energy (λ) can give an insight into the charge transfer properties of the system. The reorganization energy is a key factor controlling the rate of charge transport in a system within an incoherent charge transport method. The energy required for the structural changes of the molecule when an electron is added or removed is the internal reorganization energy, and the external reorganization energy is due to structural modifications in the surrounding medium during the electron transfer process. The molecules with small reorganization energies are in high demand due to their numerous applications in the electronic and optoelectronic industries. The internal reorganization energy for the silicenes has been calculated at B3PW91/TZVP level using the relation [43]:

$$\lambda_{\text{hole/electron}} = (E_{\pm}^* - E_{\pm}) + (E_{\text{cation/anion}}^* - E)$$

where E is the energy of neutral state in the neutral geometry, $E_{\text{cation/anion}}^*$ is the energy of the neutral state in the cationic/anionic geometry, E_{\pm} is the energy of cationic/anionic state in that geometry and E_{\pm}^* is the energy of cationic/anionic state in the neutral geometry. The reorganization energy for the silicenes in the are reported in Table 1.2. For all the silicenes the λ_{hole} value is smaller than $\lambda_{\text{electron}}$. This is an important result, since polyacenes are also known to be hole conductors. The λ_{hole} values for PAH, C_{10}H_8 , $\text{C}_{14}\text{H}_{10}$, $\text{C}_{18}\text{H}_{12}$ and $\text{C}_{22}\text{H}_{14}$ at B3LYP/6-31G** are 0.18, 0.14, 0.11 and 0.97 eV, respectively [44]. This is in good agreement with the values that we calculated for the corresponding silicon analogues Si_{10}H_8 (0.16 eV), $\text{Si}_{14}\text{H}_{10}$ (0.13 eV), $\text{Si}_{18}\text{H}_{12}$ (0.12 eV) and $\text{Si}_{22}\text{H}_{14}$ (0.10 eV). Therefore, silicenes might be considered as “*sister molecules*” to polyacenes. The reorganization energy decreases as the value of m and n increases, which can be utilized for a wide variety of applications in electronics. The λ_{hole} and $\lambda_{\text{electron}}$ values for various silicenes suggest that with the increase in the values of m and n , silicenes show amphiphilic character. The puckering in the dihedral of peripheral hexasilicene rings increases with the addition of an electron and decreases with the removal of an electron compared to the neutral species. This difference is negligible as the number of rings increase, which implies that the charges get delocalized for larger clusters.

It is important to note that bulk Si is known to exist in only sp^3 covalently link diamond-like structure, [45] which might be visualized as layers of puckered silicenes stacked over one another with the C_3 distortions arising from the additional interlayer Si–Si bonds. This is in contrast to carbon that exists additionally in the pure sp^2 graphite structure. Thus, the absence of any other allotrope of Si similar to the graphite form in carbon can be attributed to the puckering distortion that renders π -stacking interactions ineffective through the loss of planarity in each six-membered ring, and favors an sp^3 bonding environment. Also, the diamond structure of Si ensures that Si–Si interaction energies are identical both along the layer and in between the layers. To understand the interaction between the layers, the bonding energies of the interlayer structures were computed at the same level of theory. Basis set superposition error (BSSE) was corrected using the counterpoise correction (CP) method [46].

For the dimers the Si–Si bond length varies between 2.37 and 2.39 Å along the interlayer for different sized systems, which is comparable with the bulk Si–Si bond length of 2.35 Å. The Si–Si bond length in between the layers are in the range 2.38–2.47 Å. A HOMO-LUMO gap of 2–3 eV suggests semiconducting behavior for the dimers. A higher value of the HOMO–LUMO gap compared to the corresponding monomers indicates that delocalization is more in the plane. The transfer integral in between the monomers for the dimer was calculated using the relation [47, 48].

$$t_{\text{hole}} = 1/2\{E(\text{HOMO}) - E(\text{HOMO} - 1)\}$$

$$t_{\text{electron}} = 1/2\{E(\text{LUMO} + 1) - E(\text{LUMO})\}$$

Table 1.2 Binding energy per Si atom (eV), point group, HOMO-LUMO (eV), reorganization energy for silicenes of various nuclearities at B3PW91/6-31G(d) level of theory

Molecule	Average puckering angle	Binding energy/atom	HOMO-LUMO Gap	λ_{hole}	$\lambda_{\text{electron}}$
Si ₆ H ₆	33.7	-0.90	3.22	0.26	0.96
Si ₁₀ H ₈	34.3	-0.93	2.26	0.16	0.47
Si ₁₄ H ₁₀	34.4	-0.94	1.68	0.13	0.25
Si ₁₄ H ₁₀	34.8	-0.95	2.21	0.16	0.48
Si ₁₈ H ₁₂	34.3	-0.95	1.31	0.12	0.15
Si ₂₂ H ₁₄	34.3	-0.95	1.06	0.10	0.14
Si ₁₆ H ₁₀	35.0	-0.97	1.80	0.13	0.31
Si ₂₂ H ₁₂	35.2	-0.98	1.35	0.11	0.22
Si ₂₈ H ₁₄	35.2	-0.99	1.03	0.12	0.17
Si ₂₄ H ₁₂	36.7	-1.00	1.89	0.11	0.20
Si ₃₀ H ₁₄	35.4	-1.00	1.02	0.09	0.18
Si ₃₄ H ₁₆	35.2	-0.99	0.80	0.08	0.16
Si ₃₈ H ₁₆	35.4	-1.00	0.78	0.08	0.15
Si ₄₆ H ₁₈	35.5	-1.01	0.60	0.08	0.17
Si ₄₈ H ₁₈	35.5	-1.01	0.59	0.07	0.13
Si ₅₈ H ₂₀	35.6	-1.02	0.44	0.06	0.11
Si ₇₀ H ₂₂	35.6	-1.03	0.33	0.06	0.10

The binding energies, reorganization energies, HOMO-LUMO gaps and the transfer integral for the dimers are given in Table 1.3. The binding energies calculated at B3PW91 and M05-2X levels are consistent with each other, which implies that dispersion interactions do not make a significant contribution in stabilizing the silicene dimers, unlike in the carbon analogues. The structures for the stacked dimers of the monomeric layers are shown in Fig. 1.9. One clearly observes that unlike π -stacking interactions in PAH, covalent Si-Si bonding stabilizes the interlayer bonding. It is interesting to note that both the t_{hole} and t_{electron} are about 20% of that for organic molecules like TTF, TCNQ, BTQBT, benzene and naphthalene [47, 49]. The lower values of the transfer integrals arise due to smaller spacing between the valence and conduction levels as a consequence of the more diffused orbitals on silicon compared to carbon.

1.6 Reactivity of Silicene Towards Hydrogen and Band Gap Tuning

It has been already reported that the hydrogenation of a single-layer of graphene causes remarkable changes in the electronic and atomic structures, and in the trans-

Table 1.3 Binding energy of the co-facial dimers (in eV), hole and electron reorganization energies (in eV) HOMO–LUMO (eV) and hole and electron transfer integrals (in eV) for silicenes of various nuclearities at B3PW91/6-31G(d) level of theory

Dimer	Binding energy per monomer	λ_{hole}	$\lambda_{\text{electron}}$	HOMO-LUMO gap	Transfer integral (t_{hole})	Transfer integral (t_{electron})
Si ₁₂ H ₁₂	−3.6	0.27	1.51	2.0	0.05	0.08
Si ₂₀ H ₁₆	−9.2	0.90	0.35	3.1	0.15	0.17
Si ₂₈ H ₂₀	−12.3	0.76	0.34	2.8	0.11	0.03
Si ₂₈ H ₂₀	−12.0	0.56	0.28	2.5	0.19	0.21
Si ₃₂ H ₂₀	−13.0	0.52	0.15	2.3	0.15	0.019
Si ₃₆ H ₂₄	−15.7	0.64	0.27	2.6	0.03	0.05
Si ₄₄ H ₂₄	−16.6	0.56	0.16	2.0	0.04	0.06
Si ₄₄ H ₂₈	−17.1	1.16	1.36	1.8	0.03	0.07

port properties. The successful synthesis of hydrogenated graphene (graphane) was first accomplished by Elias et al. [50]. Though the hydrogenation process is reversible, the graphane formed with sp^3 hybridized carbon atoms in the lattice is stable at room temperature for many days. It is crystalline and retains the hexagonal lattice, but the periodicity is considerably shorter compared to graphene. The hydrogenation increases the energy gap in graphane and conductance becomes temperature dependent. Annealing the graphane at high temperature restores many of the fundamental properties of graphene, like metallic state, the lattice spacing and the quantum Hall effect. An earlier theoretical calculation by Sofo et al. predicted that the chair-like conformer, with hydrogen atoms bonded to carbon on both sides of the plane in an alternating manner, is more stable than a boat-like conformer in which a pair of hydrogen atoms occupy alternate positions. Graphane also has a very high volumetric and gravimetric hydrogen density, and hence has promising applications [51]. It is interesting to study the feasibility of the hydrogenation reaction of silicenes and its effect on the different properties and structure of silicene. The stability of hydrogenated silicon fullerenes has been studied by various research groups, and they are proven to have a potential hydrogen storage capacity. An efficient and low cost storage material for hydrogen is a major challenge for the current scientific community, and this is an area of active research. The US Department of Energy hydrogen storage system targeted a 6.0 weight percent gravimetric capacity and a volumetric capacity of 0.045 kg L^{−1} for the year 2010 [52]. Previous first principle calculations by Cao et al. revealed that silicon nanotubes are better candidates for hydrogen storage compared to iso-diameter carbon nanotubes. The denser and more localized electron clouds of silicon nanotubes can adsorb hydrogen more strongly [53].

The structures of silicenes with different nuclearity were optimized after saturating all the bonds with hydrogen atoms. The heat of hydrogenation is calculated using the relation $\Delta H = H(\text{Si}_a\text{H}_{b+c}) - (H(\text{Si}_a\text{H}_b) + c/2 \text{H}_2)$, where c is the number of hydrogen molecules added for complete saturation (see Fig. 1.10). The result shows that the

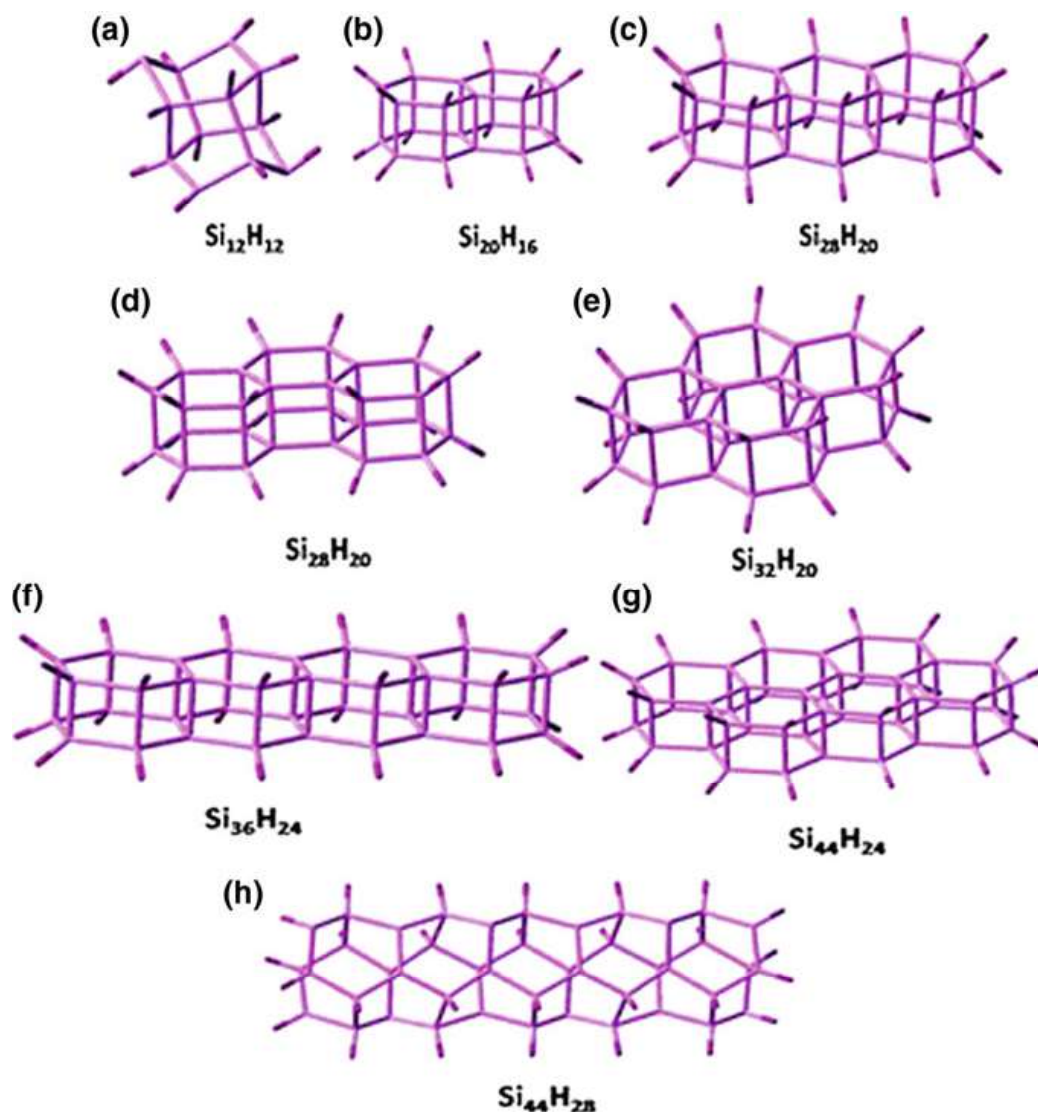


Fig. 1.9 The optimized “tiffin-box like” structures for the stacked dimers of the silicene strips at B3PW91/6-31 G(d) level of theory. Reproduced from [30] with permission from PCCP Owner Societies

reaction is more exothermic than the carbon counterparts. The heat of hydrogenation for benzene, naphthalene, anthracene and phenanthrene is -2.16 eV, 3.5 eV, 5.0 eV and 4.7 eV, respectively, [54] which in the silicon world for Si_6H_6 , Si_{10}H_8 , the anthracene analogue of Si, $\text{Si}_{14}\text{H}_{10}$ and the phenanthrene analogue of Si, $\text{Si}_{14}\text{H}_{10}$, are -4.63 , -7.48 , -10.40 and -10.25 eV. The instability of sp^2 silicon in silicene compared to sp^2 carbon in graphene makes hydrogenation more feasible in the case of silicene. The weight percent of hydrogen for various silicenes (values for carbon analogues in the parenthesis) are given in Table 1.4, and it ranges from 6.6 to 4.5%. The preference of Si to be in an sp^3 environment rather than an sp^2 environment is evident from the structural parameters. The Si–Si bond length in hydrogenated

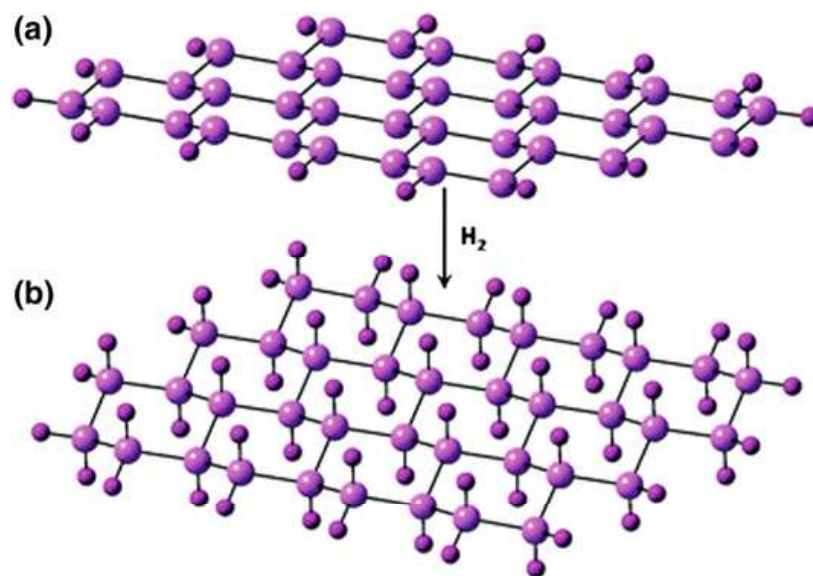


Fig. 1.10 Schematic representation of structural changes in silicene clusters on hydrogenation. Reproduced from [30] with permission from PCCP Owner Societies

silicenes is between 2.35 and 2.36 Å, which agrees well with the standard value of 2.35 Å. The Si–Si–Si bond angles are in the range 110–111°, and Si–Si–H bond angles range between 107 and 109°. The HOMO–LUMO gap and polarizability of the hydrogenated silicenes are also given in Table 1.4. All the silicenes under our study have HOMO–LUMO gaps greater than 4 eV, indicating a shift from the zero gap semiconductor realm to that of wide gap semiconductors. The increase of the band gap during saturation of silicenes with hydrogens can be used for band gap tuning by controlled saturation by hydrogen. Though the storage capacities of these clusters are comparatively lower than PAH, coupled with their band engineering properties silicenes can be seen as promising materials.

1.7 Tip Enhanced Raman Spectroscopy (TERS) as a Probe for the Buckling Distortion in Silicene

Raman spectroscopy is a significant tool for the characterization of 2D materials. The Raman spectrum of graphene has been shown to evolve with the number of layers and can be effectively used to differentiate monolayer, bilayer and multilayer graphene [55]. This non-destructive technique is also sensitive towards the quality of layers, doping level and defects in the graphene sheet [56]. Scalise et al. have calculated the Raman spectrum of free standing silicene and germanene and also the nanoribbons of Si and Ge [57]. They found that silicene shows an intense G-like peak at 570 cm^{-1} . Corresponding to the D peak in graphene, Si nanoribbons show a peak at 515 cm^{-1} . Cinquanta et al. have reported the Raman spectrum of epitaxial silicene [58]. They found that the interaction of Si atoms with the Ag(111)

Table 1.4 Heat of hydrogenation, HOMO–LUMO gap, polarizability and weight percent of H for hydrogenated silicenes (silicanes) of various nuclearities

Species	Heat of hydrogenation (eV)	Heat of hydrogenation/Si-atom	HOMO-LUMO gap (eV)	Polarizability (a.u.)	% wt. of hydrogen
Si ₆ H ₁₂	−4.63	−0.77	6.97	175.63	6.6
Si ₁₀ H ₁₈	−7.48	−0.75	5.96	307.51	6.0
Si ₁₄ H ₂₄	−10.40	−0.74	5.35	425.41	5.7
Si ₁₄ H ₂₄	−10.25	−0.73	5.54	445.59	5.7
Si ₁₈ H ₃₀	−13.34	−0.74	5.00	606.28	5.6
Si ₂₂ H ₃₆	−16.29	−0.74	4.78	766.09	5.5
Si ₁₆ H ₁₆	−11.35	−0.71	5.48	507.29	3.4
Si ₂₂ H ₃₄	−15.61	−0.71	5.01	734.18	5.2
Si ₂₈ H ₄₂	−19.77	−0.71	4.70	969.62	5.0
Si ₂₄ H ₃₆	−17.70	−0.74	5.12	798.21	5.0
Si ₃₀ H ₄₄	−20.94	−0.70	4.81	1037.82	5.0
Si ₃₄ H ₅₀	−23.95	−0.70	4.49	1214.41	5.0
Si ₃₈ H ₅₄	−26.32	−0.69	4.54	1357.97	4.8
Si ₄₆ H ₆₄	−31.68	−0.69	4.37	1690.37	4.7
Si ₄₈ H ₆₆	−32.87	−0.68	4.45	1766.55	4.7
Si ₅₈ H ₇₈	−39.46	−0.68	4.28	2189.89	4.6
Si ₇₀ H ₉₂	−47.23	−0.67	4.22	2040.75	4.5

surface distorts the low buckled silicene structure and enlarges the unit cell. The intense sharp peak at 516 cm^{-1} resembling the G-peak of graphene is a fingerprint of silicene. Calculations have been performed on free standing silicene clusters to capture the signature of buckling distortion in the Raman spectrum and enhance the intensity of this particular normal mode using metal clusters [59]. The vertical displacement of alternate Si atoms of each hexagonal ring along the C_{3v} axis leads to the buckling distortion in silicene. Since the dipole moment of the molecule is not changing during the buckling distortion, infrared (IR) spectroscopy cannot track this effect.

The vibrational frequencies and Raman intensities for various clusters of silicene were calculated. In order to examine the effect of metal clusters on Raman intensity, the silicene clusters: Si₆H₆, Si₁₄H₁₀ and the fused cluster Si₁₈H₁₂ were chosen. The clusters of gold and silver are considered to be adsorbed on the silicene surface. The M₂, M₄ and M₂₀ clusters of Au and Ag were placed at a distance of 2.5 Å from the center of mass of silicene clusters from the tip of the cluster as shown in Fig. 1.11. The distance of 2.5 Å is selected based on the most stable vertical configuration of the metal dimer (M₂). The ECP basis set LANL08(f) [60–62] available from the EMSL Basis Set Exchange Library [63, 64] was employed for the metal atoms.

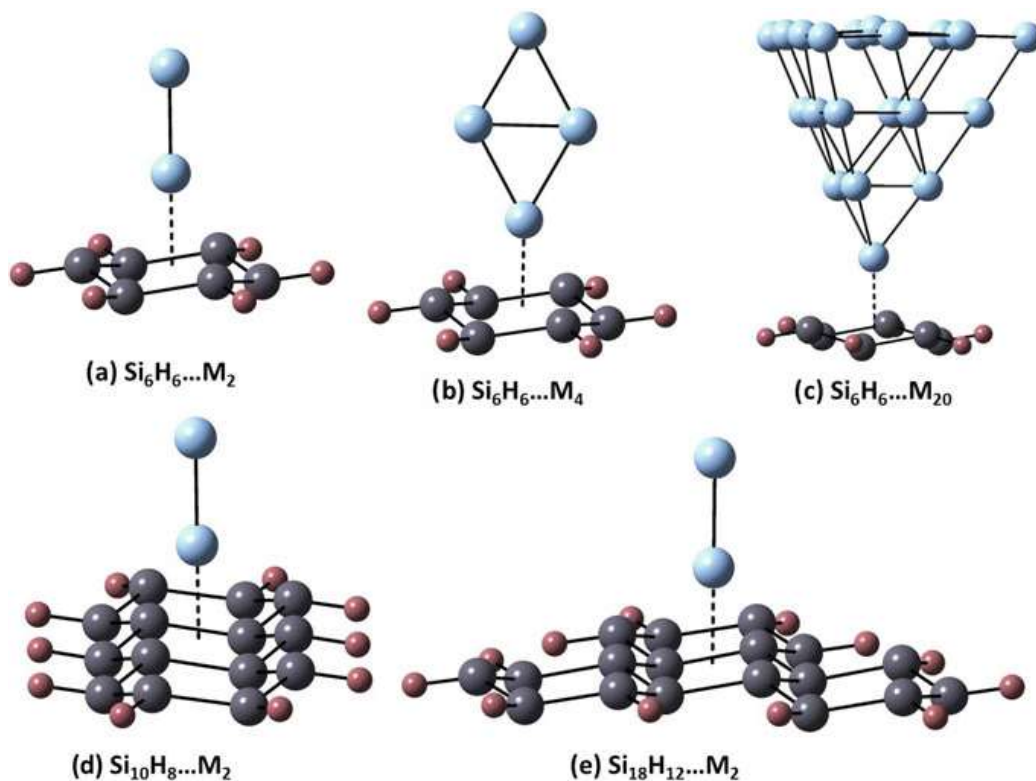


Fig. 1.11 Silicene fragments with metal clusters adsorbed over the surface ($M = \text{Au, Ag}$). Reproduced from [59] with permission from PCCP Owner Societies

The high sensitivity of surface-enhanced Raman scattering (SERS) has made it a powerful analytical technique [65–67]. The combination of scanning probe microscopy (SPM) and SERS, Tip-enhanced Raman scattering (TERS), is promising with added advantages like uniform enhancement of the signal at all sample locations, high spatial resolution, coupling of topographic features with spectroscopic data, quantitative measurement of SERS etc. [68, 69]. In TERS, the SPM tip is an externally tunable hot spot and one can effectively use it to enhance the Raman signal. Clusters of silver and gold to model the tip and study its effect on the Raman spectra of the silicene cluster. The buckling frequency, Raman scattering activity, enhancement in the scattering activity and binding energy for the silicene clusters Si_6H_6 , $\text{Si}_{14}\text{H}_{24}$ and $\text{Si}_{18}\text{H}_{12}$ in the presence of metal clusters are given in Table 1.5. The enhancement in the scattering activity is calculated as the ratio of scattering activity for the buckling mode of the silicene-metal complex to the scattering activity of the most prominent buckling mode of the corresponding silicene cluster. While, the enhancements are modest (in between 2–5 times increase), the enhancements increase with an increase in the size of the metal cluster. For example, for hexasilabenzene (Si_6H_6) the enhancement increases from 1.1 to 4 times as a gold cluster increases in size from a simple linear dimer to a tetrahedral Au_{20} . Much stronger manifestation occurs when the tip is considered to be silver. The enhancement increases from 3 times to 17 times as the size of the Ag cluster increases from 2 to 20.

Table 1.5 The buckling frequency, scattering activity, enhancement in scattering activity and binding energy for silicene fragments in the presence of metal clusters at the M05-2X/TZVP level of theory

Species	Buckling frequency (cm^{-1})	Scattering activity (S.A) ($\text{Å}^4/\text{AMU}$)	Enhancement in S.A	Binding energy (kcal mol^{-1})
$\text{Si}_6\text{H}_6\dots\text{Au}_2$	104	25.87	1.1	-26.0
$\text{Si}_6\text{H}_6\dots\text{Au}_4$	97	52.11	2.22	-22.3
$\text{Si}_6\text{H}_6\dots\text{Au}_{20}$	100	95.24	4.05	-25.4
$\text{Si}_6\text{H}_6\dots\text{Ag}_2$	100	75.28	3.21	-18.0
$\text{Si}_6\text{H}_6\dots\text{Ag}_4$	80	169.84	7.23	-14.1
$\text{Si}_6\text{H}_6\dots\text{Ag}_{20}$	109	402.08	17.1	-18.6
$\text{Si}_{14}\text{H}_{10}\dots\text{Au}_2$	139	76.75	1.36	-25.3
$\text{Si}_{14}\text{H}_{10}\dots\text{Ag}_2$	142	103.5	1.84	-17.7
$\text{Si}_{18}\text{H}_{12}\dots\text{Au}_2$	97	18.38	1.47	-22.5
$\text{Si}_{18}\text{H}_{12}\dots\text{Ag}_2$	131	91.43	1.81	-15.3

Outlook and Future Perspectives

The bottom up design of two dimensional silicon based materials from basic starting point namely silicon substituted benzene and stitching atoms with perfection along a honeycomb is challenging. Over the last decade, synthetic chemist aided by concepts of theoretical chemistry have been able to design higher order molecular fragments of fused aromatic molecules where the carbon atoms have been replaced by silicon. One should expect bigger molecular fragments with 10–15 fused six membered rings of silicon being synthesized.

Calculations and experiments have now established that unlike graphene, silicene will be buckled which is understood on the basis of Pseudo Jahn-Teller distortions in silicon systems. Computational studies predict that intercalation of cations between the silicene layers led to suppression of the buckling distortion and the graphene like structural feature can be regained. Aromatic organosilicon compounds have excellent transport properties and the band gap can be tuned by chemical functionalization. One might anticipate that rapid progress in synthesis of such molecules would provide new insights into various aspects of the rich chemistry of silicon based aromatic compounds. The possibility of depositing such molecules on bulk silicon substrates should lead to devices which can be easily integrated into existing silicon microstructures and should show superior performance under ambient conditions. Such a rational design of new materials based on molecular properties should generate excitement in the evolving area of molecular materials. A deeper understanding of the basic forces between the substrate and the molecules can minimize dissipation channels in the charge separation processes and would further augment the discovery of new phases of in two-dimensional silicon physics. Clearly, such systems provide

a possibility of synergy between chemical synthesis, computational materials design and exotic physical properties.

Acknowledgements The authors are thankful to long-term discussions in the area of molecular vibrations in silicon systems to Alexander Boldyrev, Issac B. Bersuker and G. Narahari Sastry. Funding from INSA, DST, BRNS is duly acknowledged. Computational resources of the IACS-CRAY supercomputer for many of the calculations is highly appreciated.

References

1. M. Sainsbury, *Aromatic Chemistry* (Oxford Science Publications, Oxford, 1992)
2. E. Hückel, *Z. Physik* **72**, 310 (1931)
3. E. Hückel, *Z. Physik* **70**, 204 (1931)
4. E. Hückel, *Z. Physik* **76**, 628 (1932)
5. J. Cai, P. Ruffieux, R. Jaafar, M. Bieri, T. Braun, S. Blankenburg, M. Muoth, A.P. Seitsonen, M. Saleh, X. Feng, K. Mullen, R. Fasel, *Nature* **466**, 470 (2010)
6. K. Wakita, N. Tokitoh, R. Okazaki, S. Nagase, *Angew. Chem. Int. Ed.* **39**, 634 (2000)
7. N. Tokitoh, K. Wakita, R. Okazaki, S. Nagase, P. von Ragué Schleyer, H. Jiao, *J. Am. Chem. Soc.* **119**, 6951 (1997)
8. P. Jutzi, M. Meyer, H.V.R. Dias, P.P. Power, *J. Am. Chem. Soc.* **112**, 4841 (1990)
9. N. Tokitoh, A. Shinohara, T. Matsumoto, T. Sasamori, N. Takeda, Y. Furukawa, *Organometallics* **26**, 4048 (2007)
10. Y. Tanabe, Y. Mizuhata, N. Tokitoh, *Organometallics* **29**, 721 (2010)
11. K. Abersfelder, A.J.P. White, H.S. Rzepa, D. Scheschkewitz, *Science* **327**, 564 (2010)
12. S. Nagase, H. Teramae, T. Kudo, *J. Chem. Phys.* **86**, 4513 (1987)
13. K.K. Baldrige, O. Uzan, J.M.L. Martin, *Organometallics* **19**, 1477 (2000)
14. S. Nagase, *Bull. Chem. Soc. Jpn* **87**, 167 (2014)
15. W.D. Hobey, *J. Chem. Phys.* **43**, 2187 (1965)
16. L. Blancafort, M.J. Bearpark, M.A. Robb, *Mol. Phys.* **104**, 2007 (2006)
17. I.B. Bersuker, *Chem. Rev.* **113**, 1351 (2013)
18. D. Jose, A. Datta, *J. Phys. Chem. C* **116**, 24639 (2012)
19. H. Şahin, S. Cahangirov, M. Topsakal, E. Bekaroglu, E. Akturk, R.T. Senger, S. Ciraci, *Phys. Rev. B* **80**, 155453 (2009)
20. G.G. Guzmán-Verri, L.C. Lew Yan Voon, *Phys. Rev. B* **76**, 075131 (2007)
21. I. Bersuker, *The Jahn-Teller Effect* (Cambridge University Press, 2006)
22. P. Garcia-Fernandez, I.B. Bersuker, J.E. Boggs, *J. Chem. Phys.* **124**, 044321 (2006)
23. H.J. Worner, F. Merkt, *J. Chem. Phys.* **127**, 034303 (2007)
24. Y. Liu, S. Kumari, M. Roudjane, S. Li, D.-S. Yang, *J. Chem. Phys.* **136**, 134310 (2012)
25. K. Pokhodnya, C. Olson, X. Dai, D.L. Schulz, P. Boudjouk, A.P. Sergeeva, A.I. Boldyrev, *J. Chem. Phys.* **134**, 014105 (2011)
26. A.P. Sergeeva, A.I. Boldyrev, *Organometallics* **29**, 3951 (2010)
27. T.R. Galeev, A.I. Boldyrev, *Phys. Chem. Chem. Phys.* **13**, 20549 (2011)
28. M. Houssa, G. Pourtois, V.V. Afanas'ev, A. Stesmans, *Appl. Phys. Lett.* **97**, 112106 (2010)
29. M. Ezawa, *New J. Phys.* **14**, 033003 (2012)
30. D. Jose, A. Datta, *Phys. Chem. Chem. Phys.* **13**, 7304 (2011)
31. Z. Slanina, *Chem. Phys. Lett.* **161**, 175 (1989)
32. C. Gerdes, T. Müller, *Angew. Chem. Int. Ed.* **49**, 4860 (2010)
33. T. Szilvási, T. Veszprémi, *Organometallics* **31**, 3207 (2012)
34. R.G. Pearson, *Proc. Natl. Acad. Sci.* **72**, 2104 (1975)
35. J.C. Ma, D.A. Dougherty, *Chem. Rev.* **97**, 1303 (1997)
36. D.A. Dougherty, *Science* **271**, 163 (1996)

37. C.A. Hunter, C.M.R. Low, C. Rotger, J.G. Vinter, C. Zonta, Proc. Natl. Acad. Sci. **99**, 4873 (2002)
38. S.E. Wheeler, K.N. Houk, J. Am. Chem. Soc. **131**, 3126 (2009)
39. S. Mecozzi, A.P. West, D.A. Dougherty, J. Am. Chem. Soc. **118**, 2307 (1996)
40. S. Tsuzuki, M. Yoshida, T. Uchimaru, M. Mikami, J. Phys. Chem. A **105**, 769 (2001)
41. A.D. Zdetsis, J. Chem. Phys. **127**, 214306 (2007)
42. S.A. Abraham, D. Jose, A. Datta, ChemPhysChem **13**, 695 (2012)
43. G.R. Hutchison, M.A. Ratner, T.J. Marks, J. Am. Chem. Soc. **127**, 2339 (2005)
44. J.-L. Brédas, D. Beljonne, V. Coropceanu, J. Cornil, Chem. Rev. **104**, 4971 (2004)
45. O. Marra, C. William, *Handbook of Semiconductor Silicon Technology* (1990)
46. S.F. Boys, F. Bernardi, Mol. Phys. **19**, 553 (1970)
47. J. Huang, M. Kertesz, J. Chem. Phys. **122**, 234707 (2005)
48. A. Datta, S. Mohakud, S.K. Pati, J. Mater. Chem. **17**, 1933 (2007)
49. A. Datta, S. Mohakud, S.K. Pati, J. Chem. Phys. **126**, 144710 (2007)
50. D.C. Elias, R.R. Nair, T.M.G. Mohiuddin, S.V. Morozov, P. Blake, M.P. Halsall, A.C. Ferrari, D.W. Boukhvalov, M.I. Katsnelson, A.K. Geim, K.S. Novoselov, Science **323**, 610 (2009)
51. J.O. Sofo, A.S. Chaudhari, G.D. Barber, Phys. Rev. B **75**, 153401 (2007)
52. M. Hu, X. Zhang, D. Poulidakos, Phys. Rev. B **87**, 195417 (2013)
53. J. Lan, D. Cheng, D. Cao, W. Wang, J. Phys. Chem. C **112**, 5598 (2008)
54. J.P. Lowe, K.A. Peterson, *Quantum Chemistry*, 3rd edn. (Elsevier, USA, 2006)
55. A.C. Ferrari, J.C. Meyer, V. Scardaci, C. Casiraghi, M. Lazzeri, F. Mauri, S. Piscanec, D. Jiang, K.S. Novoselov, S. Roth, A.K. Geim, Phys. Rev. Lett. **97**, 187401 (2006)
56. A.C. Ferrari, Solid State Commun. **143**, 47 (2007)
57. E. Scalise, M. Houssa, G. Pourtois, B. Broek, V. Afanas'ev, A. Stesmans, Nano Res. **6**, 19 (2013)
58. E. Cinquanta, E. Scalise, D. Chiappe, C. Grazianetti, B.V.D. Broek, M. Houssa, M. Fanciulli, A. Molle, [arXiv:1212.5422](https://arxiv.org/abs/1212.5422) [cond-mat.mes-hall]
59. D. Jose, A. Nijamudheen, A. Datta, Phys. Chem. Chem. Phys. **15**, 8700 (2013)
60. P.J. Hay, W.R. Wadt, J. Chem. Phys. **82**, 299 (1985)
61. L.E. Roy, P.J. Hay, R.L. Martin, J. Chem. Theory Comput. **4**, 1029 (2008)
62. A.W. Ehlers, M. Böhme, S. Dapprich, A. Gobbi, A. Höllwarth, V. Jonas, K.F. Köhler, R. Stegmann, A. Veldkamp, G. Frenking, Chem. Phys. Lett. **208**, 111 (1993)
63. D. Feller, J. Comput. Chem. **17**, 1571 (1996)
64. K.L. Schuchardt, B.T. Didier, T. Elsethagen, L. Sun, V. Gurumoorthi, J. Chase, J. Li, T.L. Windus, J. Chem. Inf. Model. **47**, 1045 (2007)
65. M. Moskovits, Rev. Mod. Phys. **57**, 783 (1985)
66. K. Kneipp, H. Kneipp, I. Itzkan, R.R. Dasari, M.S. Feld, Chem. Rev. **99**, 2957 (1999)
67. S.E.J. Bell, N.M.S. Sirimuthu, Chem. Soc. Rev. **37**, 1012 (2008)
68. R.M. Stöckle, Y.D. Suh, V. Deckert, R. Zenobi, Chem. Phys. Lett. **318**, 131 (2000)
69. E. Bailo, V. Deckert, Chem. Soc. Rev. **37**, 921 (2008)